# Compound prism design principles, II: triplet and Janssen prisms

Nathan Hagen[1,2] and Tomasz S. Tkaczyk[1,3]

[1]Department of Bioengineering, Rice University, Houston Texas 77005, USA

[2]e-mail: nhagen@optics.arizona.edu

[3]e-mail: ttkaczyk@rice.edu

Received 26 May 2011; accepted 5 July 2011;
posted 12 July 2011 (Doc. ID 148164); published 30 August 2011

Continuing the work of the first paper in this series [Appl. Opt. **50**, 4998–5011 (2011)], we extend our design methods to compound prisms composed of three independent elements. The increased degrees of freedom of these asymmetric prisms allow designers to achieve greatly improved dispersion linearity. They also, however, require a more careful tailoring of the merit function to achieve design targets, and so we present several new operands for manipulating the compound prisms' design algorithm. We show that with asymmetric triplet prisms, one can linearize the angular dispersion such that the spectral sampling rate varies by no more than 4% across the entire visible spectral range. Doing this, however, requires large prisms and causes beam compression. By adding a beam compression penalty to the merit function, we show that one can compromise between dispersion linearity and beam compression in order to produce practical systems. For prisms that do not deviate the beam, we show that Janssen prisms provide a form that maintains the degrees of freedom of the triplet and that are capable of up to 32° of dispersion across the visible spectral range. Finally, in order to showcase some of the design flexibility of three-element prisms, we also show how to design for higher-order spectral dispersion to create a two-dimensional spectrum. © 2011 Optical Society of America

*OCIS codes:* 230.5480, 080.2740, 260.2030, 300.6190.

## 1. Introduction

Compound prisms consist of multiple glass wedges placed in contact with one another as a single optical element. The first paper of this series [1] introduced basic design principles for doublet and double Amici compound prisms, concentrating on compact and linear-in-wavelength dispersive prisms. There we showed that it is possible to achieve a degree of dispersion previously only thought possible with gratings while maintaining direct-vision geometry. This characteristic is made possible by the underappreciated advantage that prisms have in design flexibility: with multiple surfaces and multiple glass choices available, an optical designer has several parameters to adjust for optimizing prism performance.

Here we remove the symmetry constraints of the double Amici design by designing "triplet" prisms of three independent elements, or maintaining symmetry while adding elements (Janssen prisms) [2]. The additional degrees of freedom in these designs allow for large improvements in dispersion linearity. In order to design these prisms, however, additional constraints need to be added to the design algorithm's merit function in order to produce practical designs. For example, we show that there is a direct trade-off between prism symmetry and dispersion linearity—a trade-off that also causes an unwanted compression of the transmitted beam. Balancing this beam compression against linearity thus requires adding a beam compression penalty term to the merit function. Other requirements produce additional penalty terms. Together, these tools for modifying the merit function allow a user to tailor our custom software or any commercial optical design software

0003-6935/11/255012-11$15.00/0
© 2011 Optical Society of America

to produce practical triplet and Janssen dispersive prisms.

In order to show the power of these triplet and Janssen prisms, we show prism designs for the same target values as in Paper I [1], for which we can directly compare the dispersion linearity with that achieved by doublet and double Amici systems. We also modify the design algorithm for achromatic beam steering prisms to produce higher-order dispersion, in which the spectrum can be made to wrap back on itself one or more times. This property can be used to real advantage in dual-band spectrometers, in which the spectrum from two different spectral ranges are simultaneously measured on the same detector array. One can also use higher-order dispersion together with a cross-dispersing element to achieve an echellelike two-dimensional dispersion pattern for increased spectral sampling. We show some example designs for use across the visible and near-IR spectrum.

In the third paper of this series [3], we bring together all of the methods discussed below to develop practical direct-view prism designs for the demanding application of spectral-domain optical coherence tomography systems.

## 2. Triplet Prisms

In the first paper of this series [1], we presented a method for designing doublet and double Amici prisms. While the double Amici design uses three elements, the first and third elements are identical, and thus it does not have as many degrees of freedom as a general three-element prism (such as the one shown in Fig. 1) in which all three glasses and all three apex angles are allowed to differ.

A three-glass prism has sufficient degrees of freedom that the central deviation $\bar{\delta} = \delta(\bar{\lambda})$, angular spectrum width $\Delta = \delta(\lambda_{\min}) - \delta(\lambda_{\max})$, and a third constraint can all (in principle) be satisfied exactly

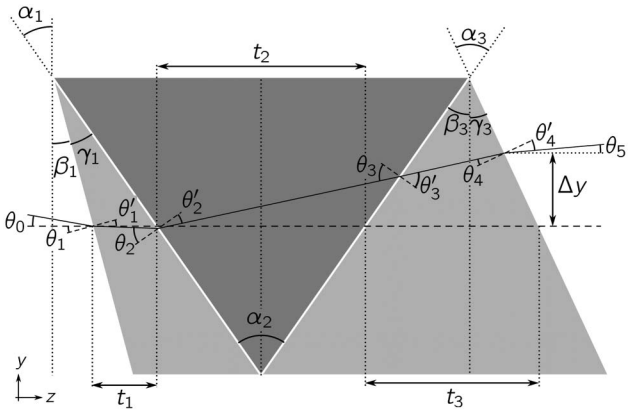


Fig. 1. Ray trace through an example triplet compound prism where the second element is assumed to be oriented symmetrically with respect to the normal to the optical axis. The system shown here has prism apex angles $(\alpha_1, \alpha_2, \alpha_3) = (20°, -70°, 60°)$, indices of refraction $(n_1, n_2, n_3) = (1.45, 1.80, 1.60)$, overall height $h$, beam displacement $\Delta y$, and axial thicknesses $t_1$, $t_2$, and $t_3$. The input ray has angle $\theta_0 = -10°$ such that $\delta = 15°$.

independent of glass choice. One can, for example, attempt a design with zero beam displacement $(\Delta y(\lambda_{\text{ref}}) = 0)$ at some reference wavelength $\lambda_{\text{ref}}$. Alternatively, the extra degrees of freedom can be used simply to further improve on the dispersion linearity or the overall system thinness.

As with the doublet and double Amici designs, one can use the small angle approximations to develop linear design equations for triplet compound prisms. If dispersion linearity is the third design target (after $\bar{\delta}^*$ and $\Delta^*$), then one method for improving dispersion linearity is to force the angular separation from the center to long wavelengths to be half that of the total spectrum angular width [4]. This allows for a linear algebra approach to a solution, as shown below. For a three-element prism, this half-angular width constraint can be represented by the equation

$$\begin{aligned}\bar{\delta} - \delta_C &= (\bar{\delta}_1 + \bar{\delta}_2 + \bar{\delta}_3) - (\delta_{C,1} + \delta_{C,2} + \delta_{C,3}) \\ &= \bar{\delta}_1\left(\frac{P_1}{V_1}\right) + \bar{\delta}_2\left(\frac{P_2}{V_2}\right) + \bar{\delta}_3\left(\frac{P_3}{V_3}\right),\end{aligned}$$

where $P$ is the relative partial dispersion, $\delta_C = \delta(\lambda_C)$, and $\lambda_C = \lambda_{\max}$ is longest wavelength. The subscripts 1, 2, and 3 represent the three elements comprising the triplet. If we write the linear approximation to the dispersion $\Delta$ as $\tilde{\Delta}$ and set $\bar{\delta} - \delta_C = \tilde{\Delta}/2$, then

$$\frac{\tilde{\Delta}}{2} = \bar{\delta}_1\frac{P_1}{V_1} + \bar{\delta}_2\frac{P_2}{V_2}.$$

At this point, if we include the linear equations for the central deviation and the total dispersion (Eqs. 3 and 4 in Paper I), we have three equations and three unknowns, namely the center wavelength deviations $\delta(\bar{\lambda})$ of each prism. Writing out the system in terms of linear equations gives

$$\begin{aligned}\begin{pmatrix}\bar{\delta}\\ \tilde{\Delta}\\ \tilde{\Delta}/2\end{pmatrix} &= \begin{pmatrix}1 & 1 & 1\\ 1/V_1 & 1/V_2 & 1/V_3\\ P_1/V_1 & P_2/V_2 & P_3/V_3\end{pmatrix}\begin{pmatrix}\bar{\delta}_1\\ \bar{\delta}_2\\ \bar{\delta}_3\end{pmatrix} \\ &= \mathbf{H}_3\begin{pmatrix}\bar{\delta}_1\\ \bar{\delta}_2\\ \bar{\delta}_3\end{pmatrix},\end{aligned}$$

so that an estimate of the central deviations of the individual prism elements is obtained by

$$\begin{pmatrix}\hat{\bar{\delta}}_1\\ \hat{\bar{\delta}}_2\\ \hat{\bar{\delta}}_3\end{pmatrix} = \mathbf{H}_3^{-1}\begin{pmatrix}\bar{\delta}\\ \tilde{\Delta}\\ \tilde{\Delta}/2\end{pmatrix},$$

giving the prism apex angles

$$\begin{pmatrix}\alpha_1\\ \alpha_2\\ \alpha_3\end{pmatrix} = \begin{pmatrix}\hat{\bar{\delta}}_1/(\bar{n}_1 - 1)\\ \hat{\bar{\delta}}_2/(\bar{n}_2 - 1)\\ \hat{\bar{\delta}}_3/(\bar{n}_3 - 1)\end{pmatrix}.$$

While the linear equations can provide a good starting point when the system requires only weak dispersion (and thus small prism angles $\alpha_i$), the above approach works well only when the target spectral dispersion is quite small. Specifying this quantitatively requires one to also define the spectral range, but one can say that, for designs using the full visible spectrum, $\Delta < 1°$ satisfies this requirement.

The nonlinear equation for the deviation angle $\delta$ of a general three-element prism is given by concatenating the refraction equations

$$\left.\begin{aligned}
&\theta_1 = \theta_0 + \beta_1, && \theta_3' = \arcsin\left(\tfrac{n_2}{n_3}\sin\theta_3\right),\\
&\theta_1' = \arcsin\left(\tfrac{1}{n_1}\sin\theta_1\right), && \theta_4 = \theta_3' - \alpha_3,\\
&\theta_2 = \theta_1' - \alpha_1, && \theta_4' = \arcsin(n_3\sin\theta_4),\\
&\theta_2' = \arcsin\left(\tfrac{n_1}{n_2}\sin\theta_2\right), && \theta_5 = \theta_4' + \gamma_3,\\
&\theta_3 = \theta_2' - \alpha_2, &&
\end{aligned}\right\}, \quad (1)$$

where $\beta_1 = \alpha_1 + \frac{1}{2}\alpha_2$, $\gamma_3 = \alpha_3 + \frac{1}{2}\alpha_2$, and $\delta = \theta_0 - \theta_5$. (See Fig. 1 for an illustration defining the angles used here.)

In order to optimize a triplet prism design, we use the same nonlinear optimization algorithm, but now perform a search over all three-glass combinations in the glass catalog. The total number of glass combinations to search is thus $T_3 = (N-1)(N-1)(N-2)$, a formula derived from the fact that the first element can be any glass except AIR, the second element can be any glass except that of the first element, and the final element can be any glass except that of the former element or AIR. For the Schott glass catalog, $N = 101$ (including air as a glass type), so that a full search requires $T_3 = 990\,000$ designs. On a standard 2 GHz desktop computer, this currently requires 18 h to perform, which can be intolerably long in many cases. If we wish to speed up the search process, we can cull the glass catalog of "similar" glasses by deleting glasses that are within a given radius in the glass chart (that is, glasses that have both similar central refractive index $n(\bar{\lambda})$ and similar dispersion $\Delta n = n(\lambda_{\min}) - n(\lambda_{\max})$). This sacrifices optimality of the design but retains most of its performance and greatly reduces the time needed to obtain a set of designs. If we select the parameters of the glass-culling algorithm to reduce the Schott catalog to 23 "unique" glasses, then $T_3 = 10,164$, and the search time is reduced to 30 min.

Up to this point, the merit functions we have been using share three basic terms, and so we can call this the "base" merit function $M_0$, where

$$M_0 = (\bar{\delta} - \bar{\delta}^*)^2 + (\Delta - \Delta^*)^2 + \Theta,$$

which involves a quadratic penalty term for errors in the central deviation $\bar{\delta}$ and the overall dispersion $\Delta$, plus a term $\Theta$ penalizing designs with interface angles that are too large:

$$\Theta = \sum_{i=1}^{I} \begin{cases} 0 & \theta_i < \theta_{\text{limit}} \\ (\theta_{\text{limit}} - \theta_i)^2 & \theta_i > \theta_{\text{limit}} \end{cases}.$$

A triplet prism contains enough degrees of freedom that one can locate a continuum of design parameters for which $M_0 = 0$. In order to minimize the nonlinearity in the dispersion, we can thus add another penalty term that selects from among the $M_0 = 0$ solutions the one that minimizes the dispersion nonlinearity. This gives the new merit function

$$M_{\text{nl}} = M_0 + w_{\text{nl}}\text{NL},$$

where $w_{\text{nl}} = 25$ is the weight of the nonlinearity term relative to those of $M_0$, and the nonlinearity operand NL is defined as

$$\text{NL} = \int \left|\frac{d^2\delta}{d\lambda^2}\right| d\lambda.$$

Table 1 shows several triplet prism designs achieving 1° and 4° of dispersion—values chosen so that the prism designs can be compared directly with the double Amici designs of Paper I. Although the algorithm allows the first and last elements to share the same apex angle and material, as in a double Amici design, none of the best-performing designs use a symmetric layout, indicating that substantial performance improvement can be achieved by deviating from the symmetry of the double Amici. Compared with the corresponding double Amici designs of Paper I (see Table 2 in Paper I [1]), the 1° and 4° designs show a twofold and fivefold improvement in $\lambda$ linearity. However, if we look at the layout for these designs [see the layout for design 1b in Fig. 2(b)], we can see that there is a trade-off in prism size as well as the introduction of large beam displacement and compression.

Note that in all tabulated data, we remove the prefixes on the glass names (i.e., N-BK7 is written as BK7) in order to keep the tables compact. In some cases, we have also abbreviated names, such as LITHOSIL-Q/LITHQ and LITHOTEC-CAF2/CAF2.

Unlike all of the prism designs up to this point, the triplet designs listed in Table 1 use *different* merit functions for each section of the table: the designs of sections (a) and (b) are optimized for best dispersion linearity, while those of section (c) are optimized for minimum thickness.

The asymmetric geometry of the layouts in section (b) is remarkably successful in reducing dispersion nonlinearity, to the extent that the spectral sampling rate of design 1b varies by only 13% across the entire spectrum. It may seem counterintuitive that the spectral sampling ratio (SSR) [1] achieved by the 4° designs is closer to 1 than that of the 1° designs, but due to nonlinearities in the dispersion, the apex angles of the 4° prisms cannot be simply scaled down by a factor of 4 to achieve 1° dispersion prisms of comparable SSR. In section (c) of the table, we see that

Table 1. Best-Performing Prism Triplets for $\theta_0 = 0$, Optimized Over the Schott Glass Catalog[a]

| | Glass 1 | Glass 2 | Glass 3 | $\alpha_1$ (deg) | $\alpha_2$ (deg) | $\alpha_3$ (deg) | $\bar{\delta}$ (deg) | $\Delta$ (deg) | NL ($\times 10^4$) | SSR | $K^b$ |
|---|---|---|---|---|---|---|---|---|---|---|---|
| merit func = linearity, $\lambda$ range = 400–700 nm, $\Delta^* = 1°$ | | | | | | | | | | | |
| 1a | LASF41 | KZFS4 | LITHQ | 46.11 | −149.52 | 100.18 | 0.000 | 1.000 | 0.095 | 1.04 | 0.04 |
| 2a | LAF34 | KZFS2 | CAF2 | 44.63 | −146.85 | 98.09 | 0.000 | 1.000 | 0.158 | 1.08 | 0.11 |
| 3a | LASF31A | KZFS4 | LITHQ | 42.28 | −145.71 | 107.20 | 0.000 | 1.000 | 0.164 | 1.09 | 0.06 |
| 4a | LASF31A | KZFS4 | CAF2 | 43.79 | −141.50 | 97.84 | −0.012 | 0.988 | 0.232 | 1.13 | 0.12 |
| 5a | LASF31A | KZFS11 | K7 | 44.11 | −150.57 | 90.21 | 0.000 | 1.000 | 0.242 | 1.12 | 0.07 |
| merit func = linearity, $\lambda$ range = 400–700 nm, $\Delta^* = 4°$ | | | | | | | | | | | |
| 1b | LAK34 | F5 | CAF2 | −80.90 | 33.52 | 68.39 | 0.005 | 3.992 | 0.281 | 1.13 | 0.20 |
| 2b | LAK33A | BASF2 | CAF2 | −79.70 | 30.10 | 70.11 | 0.000 | 4.000 | 0.283 | 1.48 | 0.21 |
| 3b | LASF43 | SF1 | CAF2 | −81.83 | 40.17 | 63.90 | −0.015 | 3.992 | 0.303 | 1.37 | 0.24 |
| 4b | LASF43 | SF1 | PK52A | −84.18 | 38.35 | 64.80 | 0.004 | 3.997 | 0.317 | 1.40 | 0.25 |
| 5b | LASF9 | SF57 | CAF2 | −85.55 | 41.09 | 63.86 | 0.003 | 4.000 | 0.412 | 1.36 | 0.27 |
| merit func = thinness, $\lambda$ range = 400–700 nm, $\Delta^* = 4°$[c] | | | | | | | | | | | |
| 1c | CAF2 | SF56A | LITHQ | 57.29 | −61.66 | 57.28 | 0.014 | 4.085 | 2.519 | 9.08 | 1.00 |
| 2c | CAF2 | SF4 | CAF2 | 57.29 | −62.34 | 57.35 | −0.005 | 3.907 | 2.271 | 8.26 | 1.00 |
| 3c | LITHQ | SF11 | LITHQ | 57.29 | −63.22 | 57.29 | 0.012 | 4.070 | 2.710 | 10.05 | 1.00 |
| 4c | LITHQ | SF56A | LITHQ | 57.29 | −63.25 | 57.29 | −0.003 | 3.929 | 2.503 | 9.74 | 1.00 |
| 5c | LITHQ | SF14 | CAF2 | 57.29 | −63.40 | 57.29 | 0.006 | 4.017 | 2.556 | 9.26 | 1.00 |

[a]All of the designs are nondeviating ($\delta^* = 0$) and constrained to interface angles of 65° or less. Figure 2 shows the dispersions of all fifteen prisms listed below.

[b]For an explanation of column $K$, see Sec. 3 below.

[c]Note that section (c) of the table uses a different merit function than the previous two sections, as indicated.

despite the added degrees of freedom available to the triplet, when searching for the most compact prisms the algorithm has selected a double Amici configuration in each case. (Designs 1c, 2c, and 5c are not exact double Amici prisms, but they differ from the latter only in selecting a neighboring glass or by adjusting slightly the prism apex angle.)

In order to see how to obtain the values reported in Table 1 from the curves in Fig. 2, one can select a curve in the figure and choose the value of the

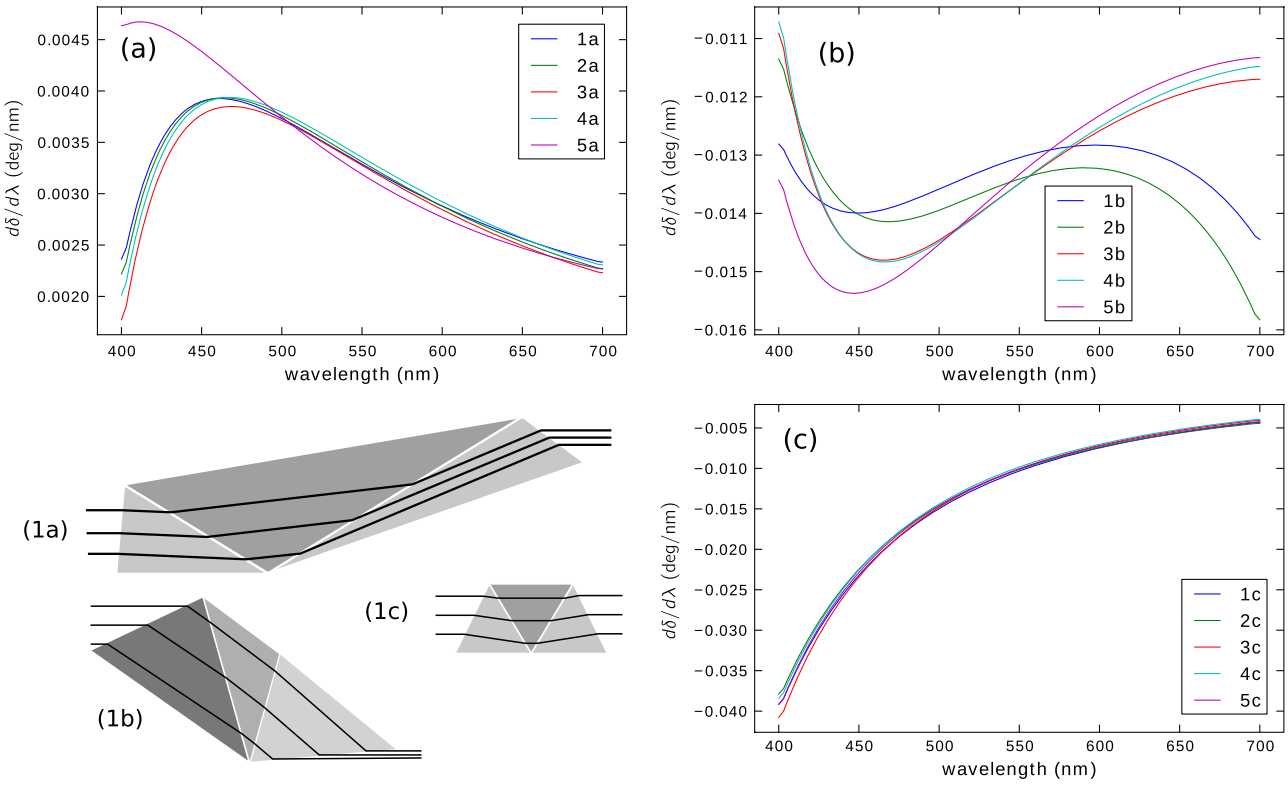


Fig. 2. (Color online) Dispersion gradients $d\delta/d\lambda$ and example layouts of the triplet designs of Table 1. Note that an ideal linear dispersion would produce a horizontal line on these plots and that the three layouts are drawn to the same relative scale.

gradient corresponding to its maximum and minimum points. The ratio of these two gives the SSR value. Since the optimization algorithm is better behaved when given quadratic error terms, the design code uses the NL value rather than SSR inside the merit function. The NL value can be obtained by first locating a least-squares fit line to the curve, and then summing the squared deviations of the curve from that line. The result is proportional to the tabulated NL values.

From Table 1 we see that the NL and SSR values do not follow one another monotonically. Since the NL operand measures the quadratic distance while the SSR operand measures the absolute deviation—quantities that are nonlinearly related—the two tend to increase and decrease together, but not monotonically. For the nonlinearity-penalized merit function $M_{\mathrm{nl}}$, we use the NL operand rather than SSR because the optimization code has better convergence behavior for a quadratic penalty than a nonquadratic one.

### 3. Constraining Beam Compression

The triplet prism layout shown in design 1b of Fig. 2 indicates a design that requires the prism to be substantially larger than the beam width and that compresses the beam to ~20% its original width. Beam compression is generally unwanted because it can produce a loss in spectral resolution due to reduction in the beam diameter, and therefore a loss of NA in the spectral spread dimension. Thus, a designer will want to compromise the dispersion linearization achieved by the asymmetric layout with a reduction in the beam compression. This can be accomplished through the addition of a quadratic penalty term to the merit function, so that the new merit function becomes $M_{\mathrm{nl-K}} = M_{\mathrm{nl}} + w_k(K-1)^2$, where $K$ is the beam compression calculated by [5]

$$K = \prod_{n=1}^{N} \frac{|\cos\theta_n|}{|\cos\theta'_n|} \tag{2}$$

and $w_k = 0.01$ is the weight of the additional term relative to those of $M_{\mathrm{nl}}$. In the formula for $K$, $N$ is the number of prism elements, and the angles $\theta_n$ and $\theta'_n$ are defined as in Fig. 1. The $(K-1)^2$ term penalizes any beam compression that deviates from the target value of $K = 1$.

Using this modified merit function and rerunning the algorithm for the same target values as in Table 1, one gets the prisms listed in Table 2. We see the effect of the additional term in the merit function in the improvement of $K$, but we also see that this has slightly weakened the improvement in the linearity, as we would expect. The designs here thus show improved performance over the equivalent double Amici (see Table 2 in Paper I [1]), but reduced linearity in comparison to the equivalent unconstrained triplet designs of Table 1. The additional constraint on $K$ also increases the algorithm's calculation time—a product of the fact that tighter constraints on the design space force the optimization iteration to make smaller steps.

For the $\Delta^* = 1°$ designs, we see that the new constraint on beam compression has improved the $K$ value, and that the designs' NL values remain better than those of the corresponding double Amici prism designs. However, for the $\Delta^* = 4°$ systems, the new constraint has actually caused the algorithm to select a double Amici layout (or something very near to one) as the best available. This implies that while the $\Delta^* = 1°$ design space has enough degrees of freedom to prevent severe trade-offs, the confined design space available to a $\Delta^* = 4°$ prism does not over this spectral range. For the larger dispersion prisms,

**Table 2. Best-Performing Prism Triplets for $\theta_0 = 0$, Optimized Over the Schott Glass Catalog[a]**

| | Glass 1 | Glass 2 | Glass 3 | $\alpha_1$ (deg) | $\alpha_2$ (deg) | $\alpha_3$ (deg) | $\bar{\delta}$ (deg) | $\Delta$ (deg) | NL ($\times 10^4$) | SSR | $K$ |
|---|---|---|---|---|---|---|---|---|---|---|---|
| merit func = $M_{\mathrm{nl-K}}$, $\lambda$ range = 400–700 nm, $\Delta^* = 1°$ | | | | | | | | | | | |
| 1a | CAF2 | LASF47 | SF2 | 87.03 | −103.46 | 92.01 | 0.000 | 1.000 | 0.177 | 2.53 | 1.00 |
| 2a | CAF2 | LASF44 | F5 | 91.03 | −101.29 | 93.27 | 0.000 | 1.000 | 0.179 | 2.63 | 1.00 |
| 3a | CAF2 | LASF46A | SF56A | 84.61 | −104.96 | 93.17 | 0.000 | 1.000 | 0.181 | 2.60 | 1.00 |
| 4a | CAF2 | LAF33 | F2 | 89.08 | −104.36 | 93.11 | 0.000 | 1.000 | 0.192 | 2.81 | 1.00 |
| 5a | CAF2 | LAF35 | BAF4 | 86.18 | −107.24 | 92.22 | 0.000 | 1.000 | 0.192 | 2.82 | 1.00 |
| merit func = $M_{\mathrm{nl-K}}$, $\lambda$ range = 400–700 nm, $\Delta^* = 4°$ | | | | | | | | | | | |
| 1b | CAF2 | LAK33A | CAF2 | 94.94 | −94.30 | 94.94 | 0.000 | 3.984 | 1.762 | 5.74 | 1.00 |
| 2b | CAF2 | LAK33A | PK52A | 94.14 | −99.17 | 94.92 | −0.004 | 3.903 | 1.766 | 5.91 | 0.99 |
| 3b | CAF2 | LASF31A | BAF4 | 92.84 | −93.87 | 92.91 | 0.000 | 3.982 | 1.785 | 6.40 | 1.00 |
| 4b | CAF2 | LAK33A | FK51A | 94.58 | −98.43 | 94.90 | −0.001 | 3.963 | 1.792 | 5.93 | 1.00 |
| 5b | CAF2 | LAF34 | CAF2 | 91.94 | −90.43 | 91.94 | 0.000 | 3.983 | 1.806 | 5.97 | 1.00 |
| merit func = $M_{\mathrm{nl-K}}$, $\lambda$ range = 475–625 nm, $\Delta^* = 4°$ | | | | | | | | | | | |
| 1c | CAF2 | LASF40 | CAF2 | 99.51 | −89.98 | 99.62 | −0.001 | 3.967 | 0.736 | 2.56 | 1.00 |
| 2c | CAF2 | LASF46A | CAF2 | 92.60 | −80.23 | 92.60 | −0.000 | 3.995 | 0.768 | 2.63 | 1.00 |
| 3c | CAF2 | LASF9 | CAF2 | 94.28 | −85.24 | 94.28 | 0.000 | 3.994 | 0.773 | 2.65 | 1.00 |
| 4c | CAF2 | LASF45 | PK52A | 96.57 | −95.55 | 96.61 | −0.001 | 3.938 | 0.777 | 2.69 | 0.99 |
| 5c | CAF2 | LASF45 | FK51A | 96.92 | −94.93 | 96.80 | −0.001 | 3.966 | 0.780 | 2.69 | 1.00 |

[a]All of the designs are nondeviating ($\delta^* = 0$) and are constrained to interface angles of 65° or less. Figure 3 shows the dispersions of all 15 prisms.

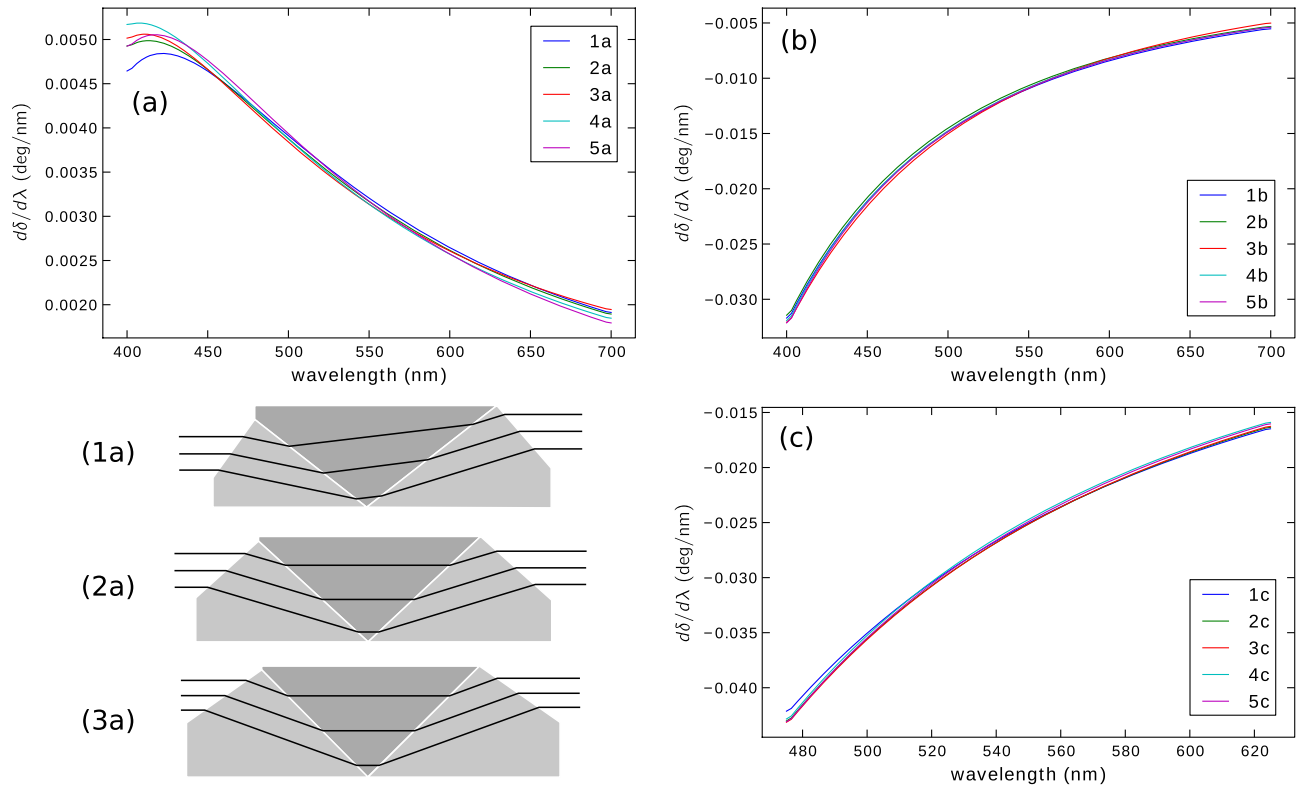


Fig. 3. (Color online) Dispersion gradients $d\delta/d\lambda$ and example layouts of the $K$-constrained triplet designs in Table 2, together with three example layouts. An ideal linear dispersion would produce a horizontal line on these plots. The layout figures were generated by replicating the design parameters in Zemax [6] and selecting the thicknesses of each prism.

the only practical means of maintaining beam size is thus to choose a symmetric layout.

Another curious feature of the 4° designs in Table 2 is the prominence of CAF2 as a glass choice. This is the least dispersive glass in the Schott glass catalog, allowing for the partial cancellation of glass dispersion nonlinearity with nonlinearity in the surface incidence angle to have maximum effect.

When designing a dispersive prism, one may want to place more emphasis on dispersion linearity versus beam compression than we have here, in which case adjusting the weight parameter $w_k$ to a smaller value will have the desired effect, producing a compromise between the designs of Table 2 and those of Table 1.

## 4. Janssen-Type Five-Element Three-Glass Symmetric Prisms

A prism designer may want to have a zero displacement system, which requires adding a penalty term proportional to $(\Delta y)^2$ to the merit function. Unfortunately, this introduces a large increase in complexity to the design algorithm, as obtaining the beam displacement value requires specifying the pupil size and location, the marginal ray angle at the pupil, and the individual thicknesses of each prism element. Rather than restricting the prism model to one angular dimension, one thus needs most of the apparatus of a full ray tracing engine in order to complete the calculation. A straightforward means of avoiding this complexity while minimizing beam displacement is to use a symmetric prism system. A double Amici is the simplest example. If we wish to take advantage of the extra degrees of freedom available to a general triplet prism, however, we can move to a five-element Janssen prism, in which two pairs of identical wedge elements surround a central element (see Fig. 4).[2]

As in the double Amici, one achieves zero beam deviation in a Janssen prism by ensuring that rays in the central element travel parallel to the optical axis. Another advantage of the increased number of elements in a Janssen prism is that dispersion can be increased beyond that achievable by a double Amici.

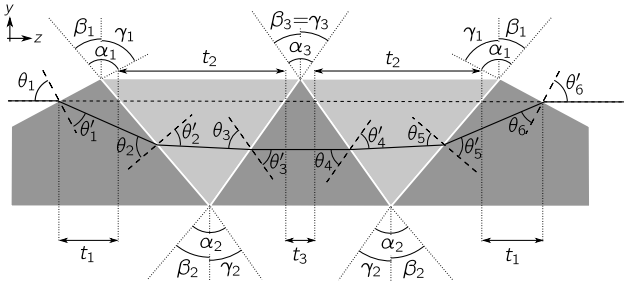


Fig. 4. Ray trace through an example Janssen prism, where the central element is assumed to be oriented symmetrically with respect to the optical axis normal. The diagram shown here has input ray angle $\theta_0 = 0°$ and a ray deviation angle $\delta = 0°$ for clarity. The beam displacement is zero, $\Delta y = 0$.

To illustrate this type of design and its potential, we once again establish the nonlinear equation for the deviation angle $\delta$ by concatenating the refraction equations

$$\left.\begin{aligned}
&\theta_1 = \theta_0 + \beta, && \theta'_4 = \arcsin\left(\tfrac{n_3}{n_2}\sin\theta_4\right),\\
&\theta'_1 = \arcsin\left(\tfrac{1}{n_1}\sin\theta_1\right), && \theta_5 = \theta'_4 - \alpha_4,\\
&\theta_2 = \theta'_1 - \alpha_1, && \theta'_5 = \arcsin\left(\tfrac{n_2}{n_1}\sin\theta_5\right),\\
&\theta'_2 = \arcsin\left(\tfrac{n_1}{n_2}\sin\theta_2\right), && \theta_6 = \theta'_5 - \alpha_5,\\
&\theta_3 = \theta'_2 - \alpha_2, && \theta'_6 = \arcsin(n_1\sin\theta_6),\\
&\theta'_3 = \arcsin\left(\tfrac{n_2}{n_3}\sin\theta_3\right), && \theta_7 = \theta'_6 + \beta,\\
&\theta_4 = \theta'_3 - \alpha_3, &&
\end{aligned}\right\}, \quad (3)$$

where $\beta = \alpha_1 + \alpha_2 + \frac{1}{2}\alpha_3$ and $\delta = \theta_0 - \theta_7$ (see Fig. 4 for an illustration defining the angles used here). With this setup, we can search for optimal designs with the same methods as those used to model triplets (see Section 2): use nonlinear optimization to locate a solution together with a brute force search over all three-glass combinations in the catalog. Table 3 shows the best-performing prisms among the resulting designs.

The prisms of Table 3 show improvements in dispersion linearity over the equivalent $K$-constrained triplet designs in Table 1, but cannot achieve the linearity achieved by the unconstrained triplets. Moreover, we see that the symmetry of the Janssen prisms has, without enforcing the beam compression constraint explicitly, maintained the beam width in all of the listed designs.

All of the designs of Table 3 use a low-dispersion glass for the outer elements, and a high-dispersion glass for the thin element, so that the central element lies somewhere between the two in its Abbe number. Taking a look at the layouts for designs 1a, 1b, and 1c shown in Fig. 5, we can see an interesting feature in the low-dispersion design (1a), where elements 2 and 4 (the thin wedges placed between the central element and the outer elements) deflect the rays by more than the outer elements do and actually change the sense of the deflection angle. Thus, the Janssen prisms do not use the added wedge elements to "soften" the ray deviation in the way that a good multielement lens design softens the bending at each surface by spreading out the ray-bending angle across multiple surfaces. Rather, the thin wedge elements *increase* the overall bending as a means of inducing a positive amount of quadratic dispersion to cancel some of the inherent negative quadratic dispersion caused by the glasses' refractive index behavior.

If we look at the layouts for the prisms in this set (see Fig. 5), we see that as we go from design 1a to 1b and 1c the dispersion requirements increase, and that the thin elements (elements 2 and 4 in the system) have less and less effect on deviating the transmitted ray, so that the system behavior comes to approach that of a double Amici design. For the higher dispersion systems, the constraints on the design space have restricted how far we can use these thin elements to improve dispersion linearity. Nevertheless, if we compare the linearity achieved by the designs of section (b) of Table 3 with the equivalent triplet designs (section (b) of Table 2), then we can see a significant improvement in NL value. Moreover, all of the Janssen prism designs have negligible beam displacement, which can be important in some applications.

One feature where the Janssen prisms completely outperform the triplet designs is in high-dispersion systems. In Paper I we explored the dispersion limits of double Amici prisms and found that we can achieve angular dispersions of up to ~23° across the visible spectrum. Performing a similar procedure for

**Table 3. Bst-Performing Janssen Prisms for $\delta^* = 0°$ and $\theta_1 = 0$ Optimized Over the Schott Glass Catalog[a]**

| | Glass 1 | Glass 2 | Glass 3 | $\alpha_1$ (deg) | $\alpha_2$ (deg) | $\alpha_3$ (deg) | $\bar{\delta}$ (deg) | $\Delta$ (deg) | NL ($\times 10^4$) | SSR | $K$ |
|---|---|---|---|---|---|---|---|---|---|---|---|
| merit func. = linearity, $\lambda$ range = 400–700 nm, $\Delta^* = 1°$ | | | | | | | | | | | |
| 1a | CAF2 | LASF40 | LAK8 | 90.57 | 12.48 | −129.12 | 0.000 | 0.998 | 0.131 | 1.94 | 1.00 |
| 2a | CAF2 | BASF2 | LAK14 | 88.88 | 10.85 | −116.08 | −0.001 | 0.997 | 0.146 | 1.91 | 1.00 |
| 3a | CAF2 | SF67 | KZFS2 | 79.35 | 2.88 | −122.58 | 0.000 | 0.998 | 0.147 | 2.07 | 1.00 |
| 4a | CAF2 | LASF40 | LAF34 | 88.58 | 17.95 | −129.78 | 0.000 | 0.998 | 0.151 | 2.02 | 1.00 |
| 5a | PK52A | LAFN7 | LAK33A | 89.95 | 10.83 | −122.57 | 0.000 | 0.997 | 0.156 | 2.29 | 1.00 |
| merit func. = linearity, $\lambda$ range = 400–700 nm, $\Delta^* = 4°$ | | | | | | | | | | | |
| 1b | CAF2 | SF6 | LASF31A | 101.78 | 13.05 | −110.29 | 0.001 | 3.998 | 0.193 | 3.38 | 1.00 |
| 2b | CAF2 | LASF9 | LASF31A | 99.88 | 20.81 | −125.26 | 0.000 | 3.999 | 0.205 | 3.56 | 1.00 |
| 3b | CAF2 | SF14 | LASF40 | 99.57 | 17.87 | −120.36 | 0.002 | 3.996 | 0.223 | 3.76 | 1.00 |
| 4b | CAF2 | SF66 | LASF41 | 98.86 | 5.18 | −101.17 | 0.000 | 3.998 | 0.241 | 4.07 | 1.00 |
| 5b | CAF2 | SF4 | LASF31A | 103.08 | 17.07 | −114.70 | 0.000 | 4.000 | 0.242 | 2.82 | 1.00 |
| merit func. = linearity, $\lambda$ range = 400–700 nm, $\Delta^* = 8°$ | | | | | | | | | | | |
| 1c | CAF2 | SF8 | LASF31A | 103.57 | 14.59 | −108.33 | 0.005 | 7.958 | 2.615 | 4.55 | 1.00 |
| 2c | FK51A | LASF44 | BAF4 | 102.02 | −101.17 | 128.30 | 0.003 | 7.971 | 2.882 | 4.90 | 1.00 |
| 3c | CAF2 | LASF44 | BAF4 | 102.53 | −90.30 | 105.53 | 0.003 | 7.971 | 2.918 | 4.84 | 1.00 |
| 4c | PK52A | LASF31A | BASF2 | 98.79 | −89.80 | 106.15 | −0.010 | 7.949 | 2.950 | 5.18 | 1.00 |
| 5c | PK51 | LASF31A | BASF2 | 98.96 | −93.75 | 111.46 | 0.000 | 7.954 | 2.981 | 5.24 | 1.00 |

[a]Dispersions and layouts of the prisms are shown in Fig. 5.

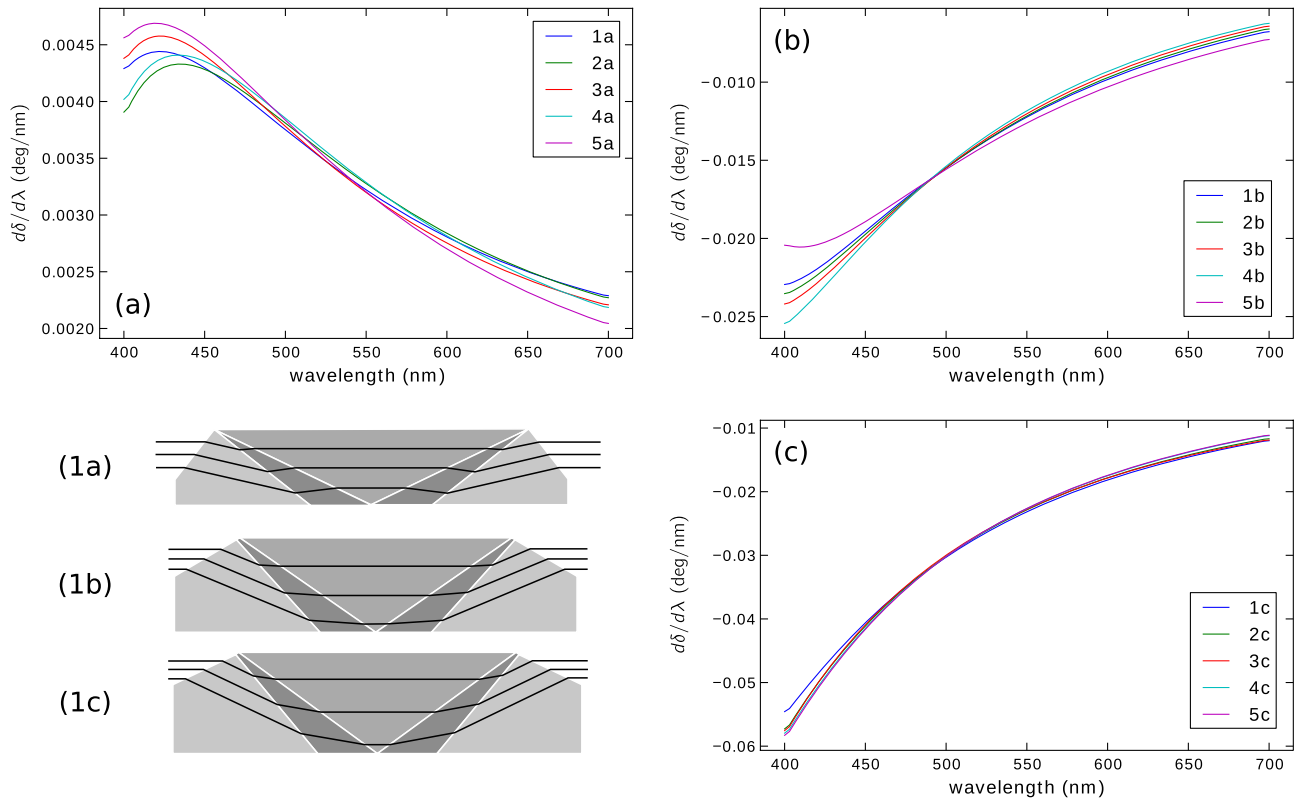


Fig. 5. (Color online) Dispersion gradients $d\delta/d\lambda$ and example layouts of the Janssen prisms shown in Table 3. An ideal linear dispersion would produce a horizontal line on these plots.

the Janssen prisms, we use the algorithm first to search for the best glass combinations for high dispersion. We then use this combination to attempt a series of prism designs for progressively greater dispersion, giving the results shown in Fig. 6. Here we see that the LAK34/SF66/LITHQ glass set can achieve up to 32.1° of dispersion (roughly equivalent to a 1400 lines/mm grating) across the 400–700 nm spectral range. Beyond 32.1°, the design algorithm fails to find a solution that can simultaneously satisfy the target values of $\bar{\delta} = 0$ and $\Delta^*$ simultaneously.

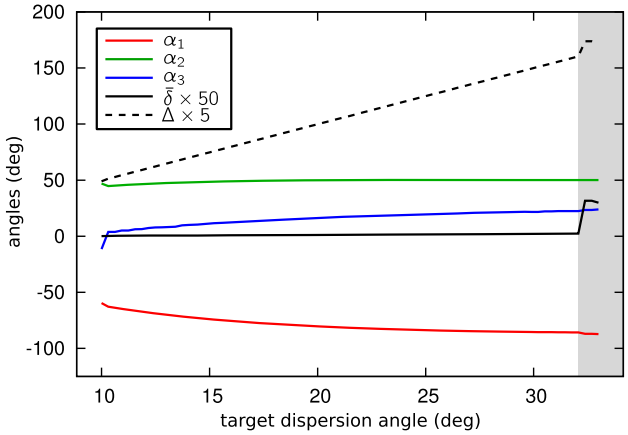


Fig. 6. (Color online) Three prism apex angles $\alpha_1$, $\alpha_2$, and $\alpha_3$, together with the central deviation $\bar{\delta}$ and total angular dispersion $\Delta$ achieved by a LAK34/SF66/LITHQ prism. Above $\Delta = 32.1°$ (indicated by the greyed region of the plot), the algorithm can no longer locate a solution that satisfies the design targets, defining the dispersion limit achievable by this glass set.

## 5. Higher-Order Spectra

In Paper I, we gave example designs of beam-steering prisms. From the plot of angular dispersion for these prisms (see Fig. 9 of Paper I), we see that the design algorithm effectively suppresses the linear and quadratic terms to the prism dispersion, leaving a cubic shape as the dominant form. In lens design, spectrum shape is commonly called "secondary spectrum" (for a quadratic form) or "tertiary spectrum" (for a cubic form). If such a prism were used in a spectrometer, the quadratic shape would cause the dispersion to start in one direction, stop, and then go back in the opposite direction, so that the spectrum folds back on itself. While this may not at first appear to be a useful property, Mooney *et al.* have shown that one can take advantage of it to design a dual-band spectrometer [7] or a spectral pseudoimager [8]. Figure 7 shows the layout, prescription (translated to our notation), and dispersion of their dual-band prism for reference.

One can also imagine inserting a cross-dispersing element together with such a second-order-dispersing prism, so that the dispersed spectrum travels twice across the width of the array in a spectrometer in a U shape, effectively doubling the sampling of the spectrum. The cubic dispersion shown in Fig. 9 of Paper I,

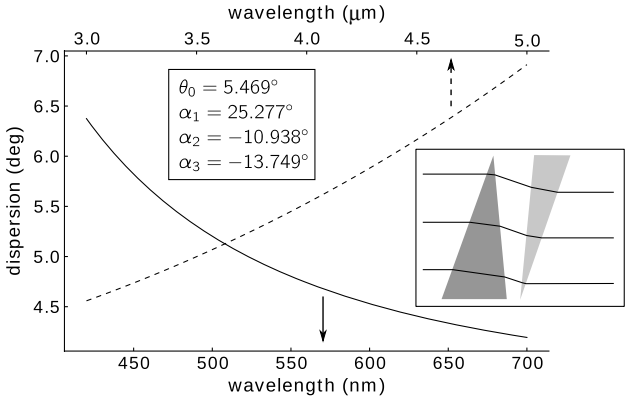


Fig. 7. Dispersion of the sapphire–air–ZnS Mooney prism over the visible and midwavelength IR bands. The prism prescription and layout are shown in boxed insets.[7]

together with a cross-dispersing element, would produce a system in which the spectrum travels three times across the length of the detector array. In this mode, such a disperser begins to resemble a low-resolution echelle system. Note that second-order dispersion is also readily achieved with a grating–prism combination in which the two dispersions are made to cancel one another at two reference wavelengths.

The higher-order dispersion shown in the beam-steering prisms of Paper I is too weak to be useful for cross-dispersing spectrometry, and so it is interesting to see if we can take advantage of compound prisms' flexibility to intentionally increase the higher-order dispersion. Nelson *et al.* describe a method of selecting glasses in order to produce a second-order spectrum that involves selecting one glass that has an absorption band just below the instrument's spectral range, and a second glass whose absorption band is just above the spectral range [8]. The two glasses have strong dispersion of opposite senses at opposite ends of the spectrum, so the combination can produce a strong higher-order spectrum. However, it can be difficult to find satisfactory glasses for a given spectral range. Instead, our approach here takes advantage of the smooth behavior of the prism design space and uses the same nonlinear algorithm to maximize the second-order component of the dispersion while maintaining target values of $\bar{\delta}$ and total dispersion $\Delta$. The merit function for this is therefore

$$M_{\mathrm{H}} = M_0 + w_{\mathrm{H}}(1/\mathrm{NL}), \tag{4}$$

where $w_{\mathrm{H}} = 0.1$ is the weight we use in our designs.

Table 4 shows ten prism designs optimized for second-order dispersion using two different spectral ranges (400 nm ≤ $\lambda$ ≤ 700 nm for section (a), 350 nm ≤ $\lambda$ ≤ 1000 nm for (b)). The resulting dispersions are shown in Fig. 8. (The reason that deviating prisms, $\bar{\delta} \neq 0$, were chosen for the designs in this table is that this greatly relaxes the design constraints, making it easier to obtain larger values for the higher-order spectra.) While this very wide spectral band is impractical for most commercial silicon-based detectors, a detector having high quantum efficiency over this entire range is possible with a deep-depletion silicon detector array.[9–11]

Each of the five designs of section (a) in the table use LASF31A (one of the highest-index glasses available) as the central element. In each design, the first element has a glass of similar dispersion to LASF31A but a lower index, while the third element uses a low-dispersion, low-index glass. In section (b), which uses a much wider spectral range, all the designs except for 4b use low-index, low-dispersion glasses exclusively for all three elements. Design 4b uses two high-index, high-dispersion glasses (SF6 and PBF2) and produces a very different high-order spectrum—one that has a large third-order component (see Fig. 8).

If used for spectrometry, the total travel of the dispersion spectrum is the main feature of interest. The travel achieved by the dispersion in the designs of Table 4 is only ~0.2° for the visible spectrum designs, but ~1.8° (0.9° in one direction and 0.9° going back) for the extended spectrum designs. Design 4b is again the exception here, as it achieves a total travel of about 2.8° (0.9° forward, 0.9° back, and 1.0° forward again).

**Table 4. Best-Performing Triplet Prisms Optimized for Second-Order Dispersion, for $\theta_0 = 0$, (a) the Schott Glass Catalog, and (b) ZEMAX's Infrared Glass Catalog**

| | Glass 1 | Glass 2 | Glass 3 | $\alpha_1$ (deg) | $\alpha_2$ (deg) | $\alpha_3$ (deg) | $\bar{\delta}$ (deg) | $\Delta$ (deg) | $\Delta_1$ (deg) | $\Delta_2$(×1000) | $\Delta_3$(×1000) |
|---|---|---|---|---|---|---|---|---|---|---|---|
| | | | | merit func = $M_2$, $\lambda$ range = 400–700 nm, $\delta^* = 45°$ | | | | | | | |
| 1a | LASF43 | LASF31A | FK51A | 84.86 | −92.21 | 84.33 | 44.997 | 0.099 | 0.003 | −0.451 | −0.054 |
| 2a | KZFS5 | LASF31A | PK51 | 92.65 | −82.46 | 78.47 | 44.998 | 0.099 | 0.015 | −0.426 | −0.386 |
| 3a | BAF52 | LASF31A | BAK4 | 95.73 | −78.41 | 72.93 | 44.997 | 0.099 | 0.020 | −0.424 | −0.483 |
| 4a | BAF52 | LASF31A | PSK3 | 94.66 | −72.26 | 66.79 | 44.996 | 0.097 | 0.025 | −0.408 | −0.565 |
| 5a | BALF5 | LASF31A | BAF52 | 98.82 | −76.41 | 71.45 | 44.998 | 0.098 | 0.021 | −0.408 | −0.312 |
| | | | | merit func = $M_2$, $\lambda$ range = 350–1000 nm, $\delta^* = 45°$ | | | | | | | |
| 1b | K10 | KZFS2 | SRF2 | 73.26 | −96.86 | 91.58 | 43.981 | 0.962 | −0.167 | 17.246 | 2.290 |
| 2b | K10 | BAF2 | SK11 | −44.31 | 121.78 | −19.04 | 44.370 | 0.896 | −0.194 | 16.394 | 2.682 |
| 3b | F_SILICA | CAF2 | BAK1 | −44.94 | 116.01 | −13.27 | 43.352 | 0.919 | −0.219 | 16.000 | 2.577 |
| 4b | SF6 | PBF2 | LAK21 | −52.83 | 96.02 | −86.01 | 44.759 | 0.967 | −0.227 | 15.644 | 4.190 |
| 5b | K10 | KZFS2 | CAF2 | −72.47 | 94.54 | −90.26 | 44.199 | 0.856 | −0.074 | 15.642 | 1.578 |

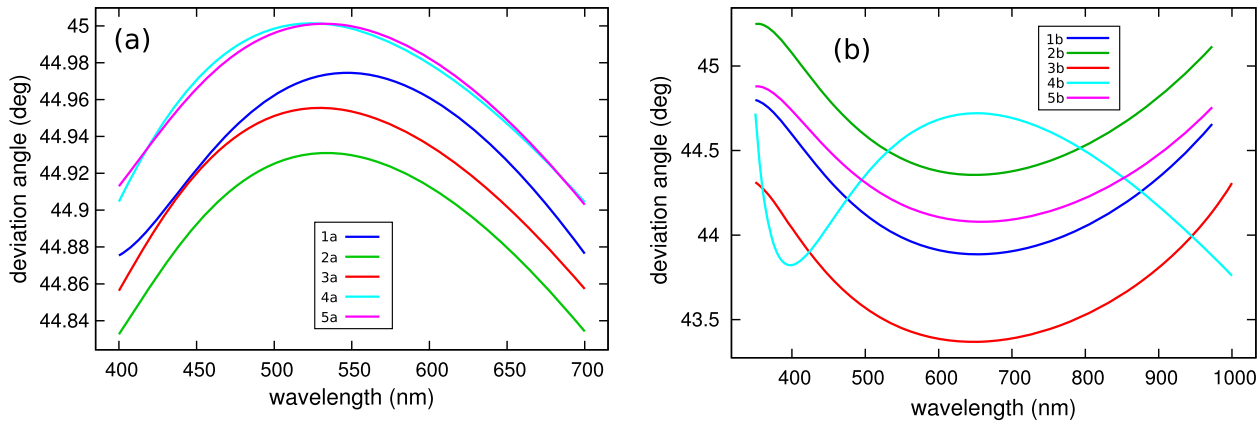


Fig. 8. (Color online) Dispersion of prisms 1a–5a and 1b–5b of Table 4.

## 6. Conclusion

Compound prisms composed of three independent elements provide remarkable power for tailoring dispersive properties. With this flexibility, however, also comes a need to constrain the design space in order to prevent unphysical or impractical solutions. The nonlinearity operand NL, beam compression operand $K$, thinness operands $A$ and $B$, chromaticity operand $C$, angle-of-incidence operand $\Theta$, and second-order operand $\Delta_2$ presented here provide a set of tools for designers to use for greatly improving on such characteristics as dispersion linearity and higher-order spectrum while minimizing negative effects on beam compression and chromaticity. The algorithm combines these with a brute force search over glass combinations, producing a long list of valid designs to choose from, among which one can then select a given prism based on alternative criteria such as cost, glass availability, a balance among the merit criteria used, etc. This allows a general method for designing linear-in-wavelength prisms, and we have shown that this can reduce the variation in spectral sampling rate across the spectrum to as low as 13% across the visible spectral range (for unconstrained triplets) or a factor of 2 (for Janssen prisms).

We have also shown how to use a penalty on beam compression to trade off unwanted changes in the beam width for a reduction in the dispersion linearity achieved. For systems in which minimization of beam displacement is also important, the symmetric double Amici and Janssen prism designs provide a simple means of achieving zero displacement. Not only can this general approach help in spectrometer design, but the same algorithms can also be applied to prism design in other applications such as beam steering and prism beam expanders (not discussed here). We have shown that the approach is even flexible enough to produce two-dimensional dispersion design (achieved by cross dispersing the high-order spectra shown in Section 5).

While all of the achievements of our customized design algorithm are possible using standard optical design software, our algorithm provides an easier interface for manipulating low-level features of the software, such as the core optimization routine and the various merit function operands, and allows use of a wide suite of numerical and text-manipulation functions available in a widely used high-level language.

Though we have mentioned some methods for reducing the calculation time of the design algorithms, the code generally requires hours in order to produce a full set of triplet or Janssen prism designs optimized over a given glass catalog (such as the Schott catalog). Since all of the code used is written in Python, one can expect an order of magnitude reduction in calculation time if the nonlinear optimization code is rewritten directly in C or Fortran.

An obvious extension of the algorithms we have shown here is to use four-glass asymmetric prisms (“quadruplets”) in order to take advantage of the even greater degrees of freedom available. Doing this blindly, however, produces an algorithm that requires weeks of computation in order to produce a full set of designs to analyze. Rather than use a brute force search through all glass combinations, as we have used up to this point, it becomes necessary to select the glasses carefully and perform optimization over a small subset of the full glass catalog. We are currently developing methods for this approach.

We encourage interested readers to download and modify the design code we have written for this work, available at the authors’ website [12].

### Appendix A: Summary of Merit Function Operands

We have used various merit functions in order to tailor compound prisms to different tasks. Here we provide a table that summarizes these operands, providing an easy means for designers to tailor their own prisms. The base merit function used throughout this series is

$$M_0 = (\bar{\delta} - \bar{\delta}^*)^2 + (\Delta - \Delta^*)^2 + \Theta.$$

With the addition of a third independent prism element, we gain the ability to further modify the merit

function without sacrificing the two target parameters in $M_0$. These additional penalty terms, along with the relative weights used in our designs, are

| Merit Function | First Term | Default Weight | Added Term |
|---|---|---|---|
| Linearity | $M_0$ | 25 | NL |
| Beam Compr. | $M_0$ | 0.0025 | $(k-1)^2$ |
| Chromaticity | $(\bar{\delta}-\bar{\delta}^*)^2$ | 1 | $C+\Theta$ |
| Thinness | $M_0$ | $0.001\Delta^*$ | $A+B$ |
| Higher-order | $M_0$ | 0.1 | 1/NL |

where the individual operands are defined as

$$A = \sum_{n}^{N} \alpha_n^2, \tag{A1}$$

$$B = \sum_{i=1}^{I} \begin{cases} (\alpha_{\text{low}} - |\alpha_i|)^2 & : \alpha_i < \alpha_{\text{low}} \\ 0 & : \alpha_i > \alpha_{\text{low}} \end{cases}, \tag{A2}$$

$$C = |\max\{\delta(\lambda)\} - \min\{\delta(\lambda)\}|, \tag{A3}$$

$$K = \prod_{n=1}^{N} \frac{|\cos\theta_n|}{|\cos\theta_n'|}, \tag{A4}$$

$$\text{NL} = \int \left|\frac{d^2\delta}{d\lambda^2}\right| \text{d}\lambda, \tag{A5}$$

$$\Theta = \sum_{i=1}^{I} \begin{cases} 0 & : \theta_i < \theta_{\text{limit}} \\ (\theta_{\text{limit}} - \theta_i)^2 & : \theta_i > \theta_{\text{limit}} \end{cases}, \tag{A6}$$

where $N$ is the number of prism elements and $I$ is the number of refractive interfaces. The $A$ operand is added to the merit function to generate thin prism designs. $B$ is used to prevent individual prism elements from becoming too thin to be practical. $C$ is the "chromaticity" term used for achromatic beam-steering prisms. $K$ is added to prevent the design from inducing excessive beam compression. NL is the term used to improve dispersion linearity. Finally, $\Theta$ is used to constrain the design space to practical elements, at which the interface angles are limited to values less than $\theta_{\text{limit}}$ (for which we have used 65° throughout both papers). The weights associated with the operands are the ones we have used for the tabulated designs and have been determined empirically. The weight for the "thinness" merit function is determined in proportion to the target dispersion because higher dispersion tends to produce larger prism angles, and thus it becomes necessary to proportionally weight the two. As an example, the exact merit function used for Table 2, with the weight terms explicitly included, is

$$M = (\bar{\delta} - \bar{\delta}^*)^2 + (\Delta - \Delta^*)^2 + \Theta^2 + 0.01(K-1)^2 + 0.1\,\text{NL}.$$

This work was partially supported by National Institutes of Health (NIH) grants RO1-CA124319 and R21-EB009186.

## References


1. N. Hagen and T. S. Tkaczyk, "Compound prism design principles, I," Appl. Opt. **50**, 4998–5011 (2011).
2. P. J. C. Janssen, "Note sur trois spectroscopes [Note on three spectroscopes]," C.R. Hebd. Seances Acad. Sci. **55**, 576–578 (1862), in French.
3. N. Hagen and T. S. Tkaczyk, "Compound prism design principles, III: linear-in-wavenumber and OCT prisms," Appl. Opt. **50**, 5023–5030 (2011).
4. E. L. Dereniak and T. D. Dereniak, *Geometric and Trigonometric Optics* (Cambridge University, 2008), pp. 347–350.
5. J. R. M. Barr, "Achromatic beam expanders," Opt. Commun. **51**, 41–46 (1984).
6. ZEMAX Development Corp. www.zemax.com.
7. J. M. Mooney, W. S. Ewing, and R. J. Nelson, "Multi-band direct vision prism," U.S. patent 6,935,757 (30 August 2005).
8. R. J. Nelson, J. M. Mooney, and W. S. Ewing, "Pseudo imaging," Proc. SPIE **6233**, 62330M (2006).
9. S. E. Holland, D. E. Groom, N. P. Palaio, R. J. Stover, and M. Wei, "Fully depleted, back-illuminated charge-coupled devices fabricated on high-resistivity silicon," IEEE Trans. Electron Devices **50**, 225–238 (2003).
10. Y. Bai, J. Bajaj, J. W. Beletic, M. C. Farris, A. Joshi, S. Lauxtermann, A. Petersen, and G. Williams, "Teledyne imaging sensors: silicon CMOS imaging technologies for x-ray, UV, visible and near infrared," Proc. SPIE **7021**, 702102 (2008).
11. S. E. Holland, W. F. Kolbe, and C. J. Bebek, "Device design for a 12.3-megapixel, fully depleted, back-illuminated, high-voltage compatible charge-coupled device," IEEE Trans. Electron Devices **56**, 2612–2622 (2009).
12. http://www.owlnet.rice.edu/~tt3/.